



Anti-correlation between Flux and Photon Index of Hard X-ray Emission from The Crab

KOOTHODIL ABHIJITH AUGUSTINE ^{1,*} AND HSIANG-KUANG CHANG ^{1,2,3,†}

¹*Institute of Astronomy, National Tsing Hua University, Hsinchu 300044, Taiwan*

²*Department of Physics, National Tsing Hua University, Hsinchu 300044, Taiwan*

³*Center for Theory and Computation (CTC), National Tsing Hua University, Hsinchu 300044, Taiwan*

ABSTRACT

Using *Swift* Burst Alert Telescope (BAT) event-mode data during Gamma Ray Burst (GRB) occurrences, we conducted spectral analysis for the Crab system. From 38 good observations, which spans over a period of 18 years from 2006 to 2023, we found that the Crab’s X-ray flux does not only flicker, but also significantly anti-correlates to its spectral power-law photon index. Since emission contribution of the Crab pulsar in this energy range is small, this anti-correlation is mainly about the emission of the Crab nebula. We suggest that this anti-correlation is an observational supporting evidence for the long-standing notion that the nebula emission is due to synchrotron radiation of shocked pulsar winds in the nebula.

Keywords: X-rays — pulsars: individual (The Crab Pulsar, PSR B0531+21) — individual (The Crab Nebula) — Photon Index and Flux — anti-correlation

1. INTRODUCTION

The Crab is one of the most widely studied ‘stable’ and bright astrophysical sources in the high energy regime. Its central pulsar, PSR B0531+21, is a rapidly rotating neutron star that emits radiation across the electromagnetic spectrum (see Bühler & Blandford (2014) and Hester (2008) for reviews on the Crab). The Crab has been used to calibrate multiple instruments in the X-ray and soft γ -ray regime (Kirsch et al. 2005).

The emission from the Crab is composed of two components: from the pulsar wind nebula (PWN) and from the pulsar. The pulsar drives electromagnetic radiation through energetic flows of electron-positron pairs, which produce the pulsar component of the emission when they are still in the magnetosphere and wind zone of the pulsar. They also create a PWN shock (forward shock) and a termination shock (reverse shock) upon interacting with the interstellar medium, leading to synchrotron emission (Slane 2017). The synchrotron radiation from electron-positron pairs in the PWN, which manifests itself as the nebula’s glow from radio to gamma-ray

bands, provides insights into particle acceleration, magnetic fields, and shock processes in the PWN (see, e.g., Arad et al. (2021) and Sironi & Cerutti (2017)). These two components, from the pulsar and from the nebula, can be distinguished through imaging or phase-resolved timing analyses, even in challenging bands like hard X-rays (e.g., Weisskopf et al. (2011); Vivekanand (2021)). It is generally believed that, in the X-ray band, the pulsar component contributes less than 20% of the total flux, with the majority coming from the PWN (Kuiper et al. 2001).

While the Crab pulsar is quite stable except for a slow, secular decrease in flux (Yan et al. 2018; Zhao et al. 2023), the nebula was found to vary at a level of a few percents and at a seeming 3-year time scale with data taken by instruments on board RXTE, *Swift*, INTEGRAL and *Fermi* in X-ray and soft gamma-ray bands from 1999 to 2010 (Wilson-Hodge et al. 2011) and *Suzaku* from 2005 to 2012 (Kouzu et al. 2013). What causes this variation is still not clear. It should be noted that the flux and spectral power-law photon index of the Crab based on NuSTAR measurements in 2015 and 2016 (Madsen et al. 2017) are in agreement with the values measured 42 years ago by Toor & Seward (1974). It suggests that the observed variability of the Crab at time scales of years is fluctuations around a steady mean. There is no indication of a long-term change up to date.

Corresponding author: Koothodil Abhijith Augustine
abhijithaugustine007@gmail.com

* abhijithaugustine007@gmail.com

† hkchang@mx.nthu.edu.tw

We report in this paper our study of the Crab’s variability using *Swift*/BAT event-mode data from 2006 to 2023. Besides the flux variation at a few percents, we found this variation is negatively correlated to its spectral power-law photon index at a statistically discernible level. Such an anti-correlation may shed some light on the cause of the observed variation. We also found that the variation time scale seems to be longer than that before year 2010.

This paper is structured as follows. First we describe the data (Section 2.1) that is used for this study and then how the data is analysed (Section 2.2). We proceed to discuss the results obtained from the analysis in Section 3. Finally, we conclude the paper in Section 4.

2. DATA

2.1. Data Selection

The *Swift* Burst Alert Telescope (BAT) is a highly sensitive, large field-of-view coded-aperture telescope designed to monitor a significant portion of the sky (2.2 steradians at a 10% coding fraction) for gamma-ray bursts (GRBs) (Barthelmy et al. 2005). When a trigger, usually a GRB, is detected, the spacecraft autonomously slews to point its two narrow-field instruments, the X-ray Telescope (Burrows et al. 2005) and the Ultraviolet Optical Telescope (Roming et al. 2005), for follow-up observations. For simplicity, we do not use data during the slew period, as it requires accounting for changes in instrumental responses during this time. Since there is ample data outside the slew period, we avoid using slew data. BAT automatically records about 1000 seconds of event data during onboard triggers. We utilize these event data (Lien et al. 2016)¹ for our analysis. We selected GRB observations by BAT that fell within a 25° field of view (FOV) of the Crab Nebula to maximize the p-code fraction. We identified 39 unique observations spanning from February 2006 to August 2023 (approximately 18 years).

The BAT’s localization accuracy is determined by the instrument’s partial coding fraction (p-code), the fraction of operational detectors exposed to a source at any given time and sky position. This p-code fraction is directly proportional to the instrument’s sensitivity and has a maximum value of 1, indicating that all available detectors are illuminated by the desired source. The importance of the partial coding fraction lies in its impact on the counts from a source (see Moss et al. (2022) for more details on p-code fraction).

2.2. Data Analysis

For data analysis, we adhered to the standard multi-step data reduction process using the HEASARC (version 6.30.1) sub-package FTOOLS, as outlined in the latest (version 6.3) BAT Guide². Background subtraction for BAT was achieved through a process called “mask weighting”. We utilized the Crab’s position (RA: 83.633114, Dec: +22.01446667) for this process (Gaia Collaboration 2020), resulting in background-subtracted light curves for the Crab. During a BAT trigger, the spacecraft will often automatically slew to the trigger location. As discussed earlier, we avoid data during the slew period and instead use data from the post-slew period, which is usually longer than the pre-slew period, increasing total source counts as the Crab moves into the BAT’s FOV from an off-axis position. This rigorous process ensured that our GTI was uncontaminated by the corresponding GRB or burst that triggered the telescope to slew and record the event data. The partial coding fraction (refer Table 1) of the Crab in all our data ranges from 0.58 to 1, indicating the Crab never lies close to the edge of the FOV in these observations. However, one observation (ID: 00234516000) did not yield any photons from the Crab after ray-tracing and was thus excluded, leaving a total of 38 observations. This careful selection process ensured that the data we analyzed was of the highest possible quality, free from significant contamination by other sources.

The spectrum of each observation was then constructed and fitted with a simple power-law model using XSPEC (Arnaud 1996) version 12.13.1. Due to BAT’s limited spatial resolution (point spread function of ~ 19.5 arcmin (Tueller et al. 2010)), the Crab is not resolved. The photon index, flux, and their chi-square values for the fitting are provided in Table 1. All errors are quoted at a 90% confidence level.

3. RESULTS

The flux and photon index obtained from the spectral fitting for all the 38 observations are plotted in Figure 1. The mean flux is $1.98_{-0.09}^{+0.04} \times 10^{-8}$ ergs/cm²/s and the mean photon index is $2.15_{-0.06}^{+0.06}$. Because of the large uncertainty, variation in the photon index cannot be confirmed statistically (fitting with a constant yielding $\chi^2_{\nu} = 0.58$). The flux variation is more significant with a constant fit yielding $\chi^2_{\nu} = 2.39$. However, they seem to vary in an opposite way. We therefore plot the flux against photon index for all observations in Figure 2 to examine their possible anti-correlation.

¹ <https://swift.gsfc.nasa.gov/results/batgrbcats/>

² https://swift.gsfc.nasa.gov/analysis/bat_swguide_v6.3.pdf

Table 1. Table of GRB and burst observations within 25-degree radius of the Crab for a period of 18 years. The partial coding fraction (which represents the quality of the observation) and χ^2 is given, for estimating the quality of the fit. GTI (Good Time Interval) is the amount of time the post-slew spectral analysis was done for. Observation with ID 00234516000 did not yield any photons while light curve was produced. The results from the spectral analysis for the remaining 38 observations are given in this table.

Observation ID	GRB or Burst	GTI (s)	p-code fraction	Start Time (MJD)	χ^2 (d.o.f = 56)	Photon Index Γ	Flux (10^{-8} erg/cm ² /s)
00180977000	GRB060210	241	0.58	53776.20	56.56	$2.16^{+0.08}_{-0.08}$	$2.20^{+0.08}_{-0.14}$
00181126000	GRB060211a	299	0.57	53777.39	49.34	$2.12^{+0.09}_{-0.08}$	$2.10^{+0.05}_{-0.13}$
00181156000	GRB060211b	238	0.94	53777.65	39.15	$2.14^{+0.07}_{-0.07}$	$2.00^{+0.05}_{-0.12}$
00284856000	GRB070714b	912	0.66	54027.17	48.32	$2.18^{+0.05}_{-0.05}$	$2.06^{+0.03}_{-0.07}$
00306793000	GRB080319d	834	0.86	54295.20	60.39	$2.13^{+0.05}_{-0.05}$	$2.02^{+0.03}_{-0.08}$
00308812000	GRB080409	785	0.99	54544.70	35.92	$2.17^{+0.05}_{-0.04}$	$2.03^{+0.04}_{-0.07}$
00321376000	GRB080822b	594	0.97	54565.05	38.53	$2.17^{+0.05}_{-0.05}$	$2.04^{+0.03}_{-0.08}$
00451191000	GRB110412a	782	0.88	54700.87	52.76	$2.24^{+0.06}_{-0.06}$	$1.90^{+0.04}_{-0.08}$
00451343000	GRB110414a	822	0.91	55663.30	43.59	$2.20^{+0.05}_{-0.05}$	$1.84^{+0.03}_{-0.07}$
00519211000	Burst (42.459, 40.466)	865	1.00	55665.31	42.07	$2.17^{+0.05}_{-0.05}$	$1.87^{+0.03}_{-0.05}$
00548927000	GRB130216a	932	0.97	56020.03	43.19	$2.12^{+0.05}_{-0.05}$	$2.07^{+0.03}_{-0.08}$
00582184000	GRB 131227A	797	0.79	56339.92	38.05	$2.13^{+0.05}_{-0.06}$	$2.11^{+0.06}_{-0.09}$
00597722000	GRB140430a	334	0.81	56653.19	41.35	$2.12^{+0.08}_{-0.07}$	$2.10^{+0.05}_{-0.12}$
00614390000	Burst (76.734, 12.820)	942	0.99	56777.85	54.36	$2.08^{+0.05}_{-0.05}$	$2.05^{+0.03}_{-0.06}$
00615399000	GRB141015a	206	0.98	56934.96	56.85	$2.11^{+0.08}_{-0.08}$	$2.02^{+0.04}_{-0.10}$
00629578000	GRB150203a	1110	0.97	56945.37	47.59	$2.21^{+0.05}_{-0.04}$	$1.94^{+0.02}_{-0.06}$
00655262000	GRB150911a	1686	0.82	57056.16	54.64	$2.20^{+0.06}_{-0.05}$	$1.90^{+0.03}_{-0.08}$
00667392000	GRB151215a	259	0.78	57276.77	44.48	$2.22^{+0.09}_{-0.09}$	$1.87^{+0.07}_{-0.15}$
00669319000	GRB160104a	780	0.92	57371.11	51.86	$2.20^{+0.05}_{-0.05}$	$1.97^{+0.03}_{-0.08}$
00676595000	Burst (107.316, 26.932)	830	0.69	57391.46	60.9	$2.22^{+0.06}_{-0.05}$	$1.92^{+0.04}_{-0.07}$
00680017000	GRB160321A	859	0.84	57446.72	60.9	$2.22^{+0.06}_{-0.05}$	$1.92^{+0.03}_{-0.08}$
00706052000	Burst (98.821, -6.645)	237	0.96	57468.65	41.55	$2.23^{+0.08}_{-0.08}$	$1.85^{+0.04}_{-0.08}$
00709765000	Burst (80.088, 40.029)	795	1.00	57595.05	65.67	$2.17^{+0.05}_{-0.05}$	$1.86^{+0.04}_{-0.09}$
00716127000	GRB161007a	840	0.77	57624.96	66.49	$2.20^{+0.05}_{-0.05}$	$1.93^{+0.04}_{-0.06}$
00820347000	Burst (66.024, 13.398)	862	0.78	57668.88	46.2	$2.15^{+0.05}_{-0.05}$	$2.03^{+0.03}_{-0.08}$
00824063000	Burst (95.957, 12.811)	790	0.90	58208.17	54.34	$2.17^{+0.05}_{-0.05}$	$2.04^{+0.04}_{-0.07}$
00853882000	Burst (104.225, 39.315)	764	0.81	58218.32	42.88	$2.10^{+0.06}_{-0.06}$	$2.09^{+0.04}_{-0.08}$
00865036000	Burst (64.746, 15.213)	823	0.79	58348.51	46.27	$2.14^{+0.06}_{-0.06}$	$2.06^{+0.05}_{-0.09}$
00927345000	Burst (86.368, -15.907)	306	0.74	58393.47	47.5	$2.10^{+0.08}_{-0.08}$	$2.07^{+0.08}_{-0.14}$
00995004000	GRB200907b	767	0.98	58757.71	41.55	$2.16^{+0.06}_{-0.06}$	$1.91^{+0.06}_{-0.08}$
01032183000	Burst (72.266, 7.269)	209	0.92	59099.77	49.57	$2.10^{+0.09}_{-0.09}$	$2.03^{+0.07}_{-0.17}$
01036227000	GRB210308a	631	0.83	59257.17	43.22	$2.11^{+0.07}_{-0.07}$	$2.07^{+0.05}_{-0.09}$
01073893000	GRB210919a	1305	0.98	59281.26	50.68	$2.16^{+0.06}_{-0.06}$	$2.03^{+0.03}_{-0.07}$
01090472000	GRB211221A	917	0.64	59476.01	46.85	$2.03^{+0.07}_{-0.07}$	$1.66^{+0.04}_{-0.11}$
01104692000	GRB220430a	725	0.83	59699.57	39.09	$2.17^{+0.06}_{-0.06}$	$1.82^{+0.04}_{-0.10}$
01104842000	Burst (85.577, 14.033)	541	0.89	59700.82	61.33	$2.18^{+0.07}_{-0.07}$	$1.92^{+0.04}_{-0.10}$
01125809000	GRB220930a	761	0.79	59852.45	45.96	$2.13^{+0.06}_{-0.06}$	$2.08^{+0.05}_{-0.12}$
01182085000	Burst (76.240, 19.561)	761	0.99	60158.27	41.15	$2.14^{+0.06}_{-0.05}$	$1.97^{+0.03}_{-0.07}$

Apparently in Fig. 2 one can see two outliers, at the lowest and highest flux among the 38 data points respectively. These two outliers are from observations of ID 01104692000 (outlier 1) and ID 00180977000 (out-

lier 2). The Spearman correlation coefficient of this distribution, when outlier 1 is excluded, is -0.70 with a p-value of 1.63×10^{-6} . It indicates a quite strong anti-correlation. When outlier 2 is also excluded, the

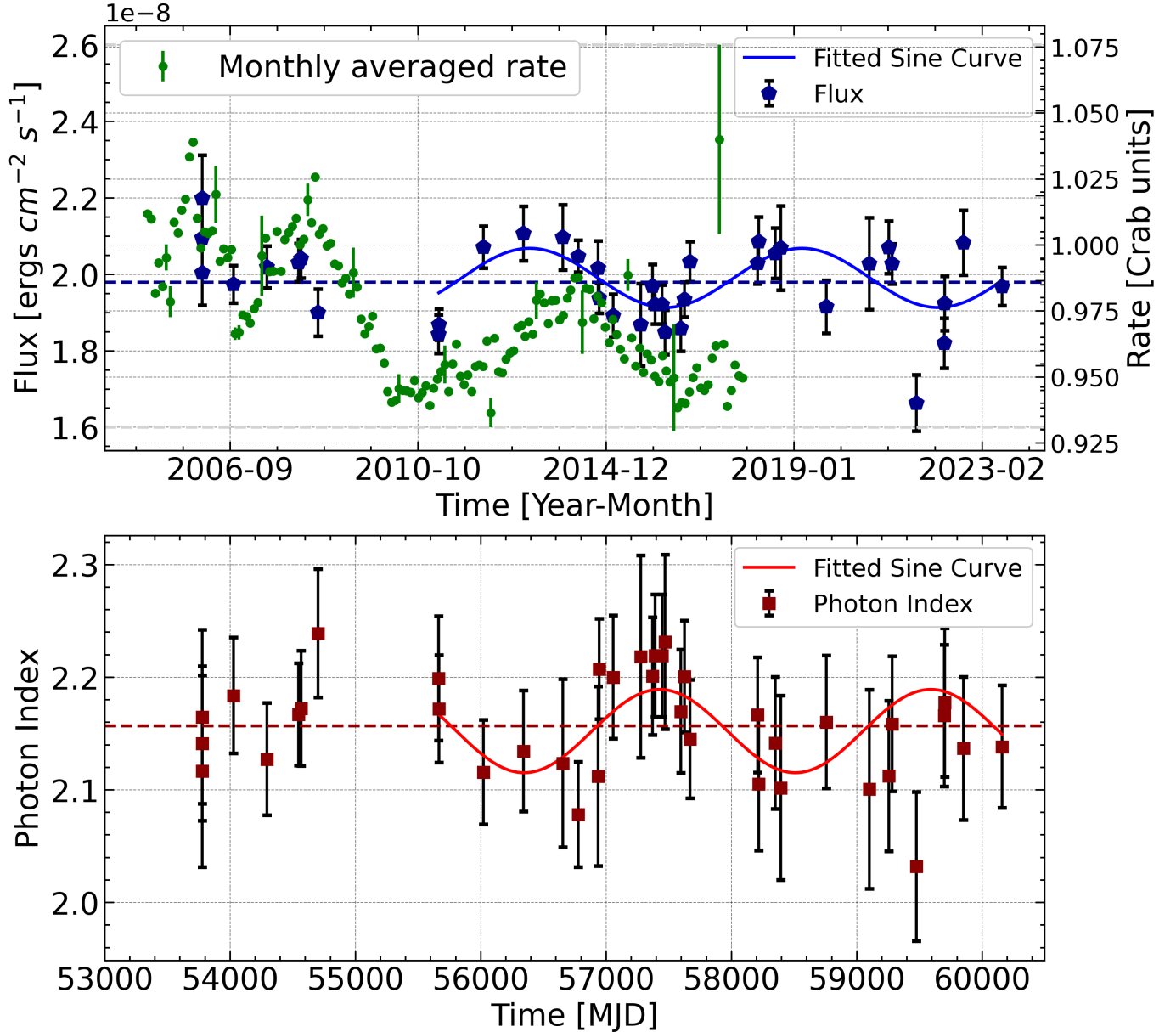


Figure 1. The Crab flux and photon index over 18 Years (February 2006 to August 2023) measured by *Swift* BAT (15-150 keV). The upper panel shows the flux and lower panel shows the photon index. Time is given in MJD and years. The dashed lines indicate the average flux and the average photon index of the 38 good observations. The green points represent the count rate in Crab units sourced from the publicly available ‘Swift BAT 157-Month Hard X-ray Survey’. The two sinusoidal curves are the best-fit sinusoidal models to the data after year 2010, excluding the outlier at MJD 59476.

Spearman correlation coefficient becomes -0.72 with a p-value of 6.29×10^{-7} .

The Crab count rate taken from the publicly available ‘Swift BAT 157-Month Hard X-ray Survey’³ is also plotted in Fig. 1. It shows the variation time scale changed after year 2010, consistent with the flux we derived from *Swift*/BAT event data. To describe the variation time

scale after 2010, we use a sinusoidal function to fit the flux and photon index, excluding outlier 1. The best-fit period for flux is 5.92 year ($\chi^2_\nu = 1.33$ with a p-value of 0.12) and that for the photon index is 5.94 year ($\chi^2_\nu = 0.37$). The time scale is about two times longer than that before 2010 (Wilson-Hodge et al. 2011). These two best-fit curves also clearly show the anti-correlation.

³ <https://swift.gsfc.nasa.gov/results/bs157mon/287>

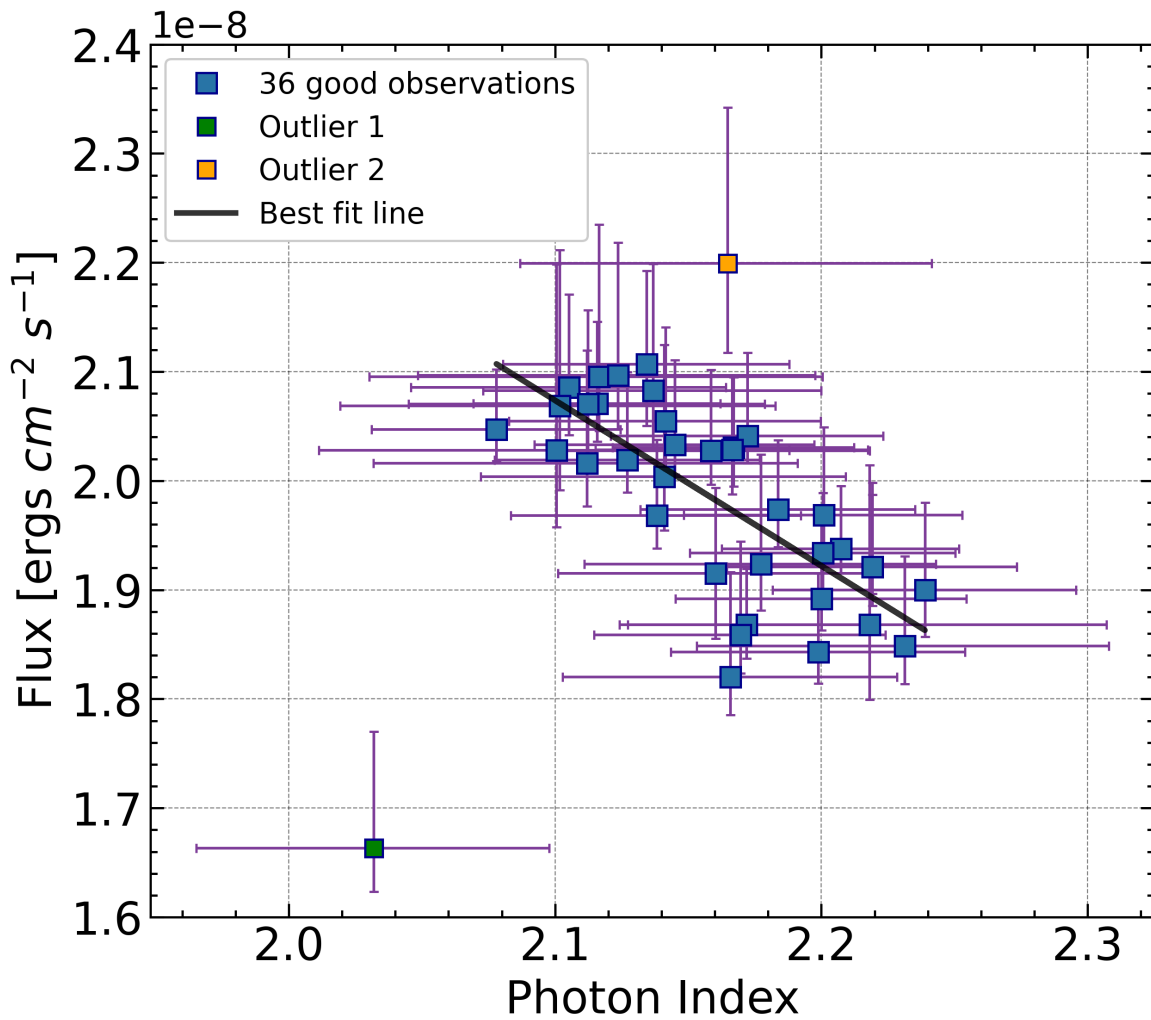


Figure 2. Flux versus photon index for all the 38 BAT (15-150 keV) observations. Two outliers are marked in different colors. The black line is the best linear fit of these data points, excluding both outliers.

Electromagnetic radiation of the Crab nebula, from radio to GeV gamma-ray bands, is usually considered to be due to synchrotron radiation because of its non-thermal spectral shape and high degree of polarization. That beyond GeV energy is attributed to coming from inverse Compton scattering between those synchrotron radiation photons (plus cosmic microwave background) and relativistic pair plasma in the pulsar winds. The synchrotron component, however, has a photon index increasing with energy, that is, softer towards higher energy bands. That, in turn, requires the radiating electrons to have corresponding power indices in their energy distribution, also increasing with energy. There are still many unsolved issues as for how to accelerate electrons to that kind of distribution (Arad et al. 2021; Sironi & Cerutti 2017). Nonetheless, no matter whether pulsar winds are energized on the way before reaching the termination shock by magnetic reconnection (Pétri 2012) or turbulent magnetic relaxation (Zrake & Arons

2017) in the striped pulsar winds, shock acceleration at the termination shock should still be at work to form non-thermal populations of relativistic electrons, which emit the observed synchrotron radiation.

The major finding of this study, that is, the anti-correlation between hard X-ray flux of the Crab and its spectral photon index, is likely a manifestation of synchrotron radiation due to particles accelerated by diffusive shock acceleration (DSA) in the PWN. On one hand, relativistic electrons of a power-law energy distribution, $N_{E,e} \propto E^{-p}$ can lead to a power-law synchrotron radiation of $F_\nu \propto \nu^{-(\frac{p-1}{2})}$, or, put in the photon number flux density format, $N_{E,\gamma} \propto E^{-(\frac{p-1}{2})-1} = E^{-(\frac{p+1}{2})} = E^{-\Gamma}$, where $\Gamma = \frac{p+1}{2}$ is the photon index. Moreover, DSA may create a power-law energy distribution of electrons described as (Eq. (17.30) in Longair (2011))

$$N_{E,e} \propto E^{-(1-\frac{\ln P}{\ln \beta})}, \quad (1)$$

where P is the probability of particle remaining in the acceleration region after one collision and β is the multiplicity for energy gain after one collision. We therefore have the power index p in the energy distribution of electrons to be $p = 1 - \frac{\ln P}{\ln \beta} = 1 + \frac{|\ln P|}{\ln \beta}$, noting that $P < 1$ and $\beta > 1$. On the other hand, change in the synchrotron radiation flux may be due to change in the radiating particle flux or in the magnetic field strength. The latter actually provides a possible link to the change of the photon index. When field strength increases, not only radiation flux increases but also the remaining probability P in Eq.(1) increases because of magnetic irregularity or turbulence with increased field strength. The energy multiplicity factor β is probably not sensitive to the magnetic field strength. With a larger P , the power index p of the electron energy distribution is smaller, and so is the radiation photon index Γ . The synchrotron radiation flux is therefore anti-correlated with its photon index if the energetic electrons are accelerated by DSA and the change is due to magnetic field strength change.

The magnetic fields around PWN shock fronts are compressed interstellar fields in the course of the nebula expansion. These fields may have been modulated in some way by the Crab supernova ejecta, which are considered to have dispersed into the interstellar medium. The details of this modulation is not clear, but we noticed that the X-ray flux variation shows a roughly 3-year timescale before April 2010, when a deeper drop in flux occurred and after which the variation timescale seems to lengthen (Figure 8 in Oh et al. (2018)). The new timescale is about 6 years, as can be seen in Figure

1. These timescales might be relic of earlier ejecta-ISM interactions.

The anti-correlation of X-ray flux and photon index in 15 keV – 150 keV we report here has actually already revealed itself in the upper panel of Figure 2 in Kouzu et al. (2013) with a positive correlation between spectral hardness and count rates using Suzaku data. This anti-correlation supports the idea that the hard X-ray emission from the Crab is synchrotron radiation of energetic electrons accelerated by DSA and the variation is due to magnetic field strength change around the shock front. The flux and spectral variation in the emission from the Crab nebula probably does not appear only in the hard X-ray regime. At higher energies, the Crab is not spatially resolved and the pulsar contribution to the whole (nebula plus pulsar) emission increases with energy (Kuiper et al. 2001). It is therefore not easy to examine this variation. On the other hand, in soft X-rays or lower energy bands, the Crab can be resolved and the nebula dominates the whole emission. Similar studies in other energy bands are very much desired. In addition, the polarization degree of these emissions may also vary in a way positively correlated to the variation of the photon index. This may be verified in soft X-rays by IXPE in the near future (Bucciantini et al. 2023).

This work is supported by the National Science and Technology Council (NSTC) of the Republic of China (Taiwan) under grant 112-2112-M-007-053. The results presented here are obtained by using the data obtained by the BAT on the *Swift* observatory by NASA with the participation of Italy and the UK. We are very much grateful to Amy Lien of the University of Tampa for her help in data processing of this work.

REFERENCES

- Arad, O., Lavi, A., & Keshet, U. 2021, MNRAS, 504, 4952, doi: [10.1093/mnras/stab1044](https://doi.org/10.1093/mnras/stab1044)
- Arnaud, K. A. 1996, in Astronomical Society of the Pacific Conference Series, Vol. 101, Astronomical Data Analysis Software and Systems V, ed. G. H. Jacoby & J. Barnes, 17
- Barthelmy, S. D., Barbier, L. M., Cummings, J. R., et al. 2005, SSRv, 120, 143, doi: [10.1007/s11214-005-5096-3](https://doi.org/10.1007/s11214-005-5096-3)
- Bucciantini, N., Ferrazzoli, R., Bachetti, M., et al. 2023, Nature Astronomy, 7, 602, doi: [10.1038/s41550-023-01936-8](https://doi.org/10.1038/s41550-023-01936-8)
- Bühler, R., & Blandford, R. 2014, Reports on Progress in Physics, 77, 066901, doi: [10.1088/0034-4885/77/6/066901](https://doi.org/10.1088/0034-4885/77/6/066901)
- Burrows, D. N., Hill, J. E., Nousek, J. A., et al. 2005, SSRv, 120, 165, doi: [10.1007/s11214-005-5097-2](https://doi.org/10.1007/s11214-005-5097-2)
- Gaia Collaboration. 2020, VizieR Online Data Catalog: Gaia EDR3 (Gaia Collaboration, 2020), doi: [10.26093/cds/vizier.1350](https://doi.org/10.26093/cds/vizier.1350)
- Hester, J. J. 2008, ARA&A, 46, 127, doi: [10.1146/annurev.astro.45.051806.110608](https://doi.org/10.1146/annurev.astro.45.051806.110608)
- Kirsch, M. G., Briel, U. G., Burrows, D., et al. 2005, in Society of Photo-Optical Instrumentation Engineers (SPIE) Conference Series, Vol. 5898, UV, X-Ray, and Gamma-Ray Space Instrumentation for Astronomy XIV, ed. O. H. W. Siegmund, 22–33, doi: [10.1117/12.616893](https://doi.org/10.1117/12.616893)
- Kouzu, T., Tashiro, M. S., Terada, Y., et al. 2013, PASJ, 65, 74, doi: [10.1093/pasj/65.4.74](https://doi.org/10.1093/pasj/65.4.74)
- Kuiper, L., Hermsen, W., Cusumano, G., et al. 2001, A&A, 378, 918, doi: [10.1051/0004-6361:20011256](https://doi.org/10.1051/0004-6361:20011256)
- Lien, A., Sakamoto, T., Barthelmy, S. D., et al. 2016, ApJ, 829, 7, doi: [10.3847/0004-637X/829/1/7](https://doi.org/10.3847/0004-637X/829/1/7)

- Longair, M. S. 2011, *High Energy Astrophysics*, 3rd edn. (Cambridge University Press),
doi: <https://doi.org/10.1017/CBO9780511778346>
- Madsen, K. K., Forster, K., Grefenstette, B. W., Harrison, F. A., & Stern, D. 2017, *ApJ*, 841, 56,
doi: [10.3847/1538-4357/aa6970](https://doi.org/10.3847/1538-4357/aa6970)
- Moss, M., Lien, A., Guiriec, S., Cenko, S. B., & Sakamoto, T. 2022, *ApJ*, 927, 157, doi: [10.3847/1538-4357/ac4d94](https://doi.org/10.3847/1538-4357/ac4d94)
- Oh, K., Koss, M., Markwardt, C. B., et al. 2018, *ApJS*, 235, 4, doi: [10.3847/1538-4365/aaa7fd](https://doi.org/10.3847/1538-4365/aaa7fd)
- Pétri, J. 2012, *MNRAS*, 424, 605,
doi: [10.1111/j.1365-2966.2012.21238.x](https://doi.org/10.1111/j.1365-2966.2012.21238.x)
- Roming, P. W. A., Kennedy, T. E., Mason, K. O., et al. 2005, *SSRv*, 120, 95, doi: [10.1007/s11214-005-5095-4](https://doi.org/10.1007/s11214-005-5095-4)
- Sironi, L., & Cerutti, B. 2017, in *Astrophysics and Space Science Library*, Vol. 446, *Modelling Pulsar Wind Nebulae*, ed. D. F. Torres, 247,
doi: [10.1007/978-3-319-63031-1_11](https://doi.org/10.1007/978-3-319-63031-1_11)
- Slane, P. 2017, *Pulsar Wind Nebulae* (Cham: Springer International Publishing), 2159–2179,
doi: [10.1007/978-3-319-21846-5_95](https://doi.org/10.1007/978-3-319-21846-5_95)
- Toor, A., & Seward, F. D. 1974, *AJ*, 79, 995,
doi: [10.1086/111643](https://doi.org/10.1086/111643)
- Tueller, J., Baumgartner, W. H., Markwardt, C. B., et al. 2010, *ApJS*, 186, 378, doi: [10.1088/0067-0049/186/2/378](https://doi.org/10.1088/0067-0049/186/2/378)
- Vivekanand, M. 2021, *A&A*, 649, A140,
doi: [10.1051/0004-6361/202140358](https://doi.org/10.1051/0004-6361/202140358)
- Weisskopf, M. C., Tennant, A. F., Yakovlev, D. G., et al. 2011, *ApJ*, 743, 139, doi: [10.1088/0004-637X/743/2/139](https://doi.org/10.1088/0004-637X/743/2/139)
- Wilson-Hodge, C. A., Cherry, M. L., Case, G. L., et al. 2011, *ApJL*, 727, L40, doi: [10.1088/2041-8205/727/2/L40](https://doi.org/10.1088/2041-8205/727/2/L40)
- Yan, L. L., Ge, M. Y., Lu, F. J., et al. 2018, *ApJ*, 865, 21,
doi: [10.3847/1538-4357/aad911](https://doi.org/10.3847/1538-4357/aad911)
- Zhao, H.-S., Ge, M.-Y., Li, X.-B., et al. 2023, *Radiation Detection Technology and Methods*,
doi: [10.1007/s41605-023-00392-2](https://doi.org/10.1007/s41605-023-00392-2)
- Zrake, J., & Arons, J. 2017, *ApJ*, 847, 57,
doi: [10.3847/1538-4357/aa826d](https://doi.org/10.3847/1538-4357/aa826d)